A Numerical Modeling Study of the Propagation of Idealized Sea-Breeze Density Currents*

F. J. ROBINSON

Department of Geology and Geophysics, Yale University, New Haven, Connecticut

M. D. PATTERSON

Department of Architecture and Civil Engineering, University of Bath, Bath, United Kingdom

S. C. SHERWOOD

Climate Change Research Centre, and ARC Centre of Excellence for Climate System Science, University of New South Wales, Sydney, New South Wales, Australia

(Manuscript received 8 April 2012, in final form 21 September 2012)

ABSTRACT

Sea breezes are often modeled as a wave response to transient heating in a stratified environment. They occur, however, as density currents with well-defined fronts, the understanding of which rests primarily on experiments and theory that do not include the stratification within and above the current and the steady heat input at the land surface. These gaps are investigated here via a sequence of idealized 2D density current simulations, progressing from the simplest classical case to more realistic surface heating and stratification.

In the classical situation where the entire horizontal density contrast is imposed initially, the front quickly attains a constant speed determined by traditional formulas based on the density contrast across the front and the current depth, or by the amount of heat needed to produce it from an initially barotropic fluid. However, these diagnostic and prognostic tools fail completely if the current is driven by a gradual input of heat, analogous to a real sea-breeze situation. In this case the current accelerates slowly at first, remaining much slower than would be expected based on classical formulas.

The motion of a classical density current is mostly inertial, with accelerations occurring at the current head; while in the continuously heated case, the entire current accelerates, requiring interior body forces to develop slowly owing to heating of the density current itself. This explains why observed sea-breeze fronts propagate more slowly than predicted from classical formulas, and may help to explain why larger landmasses, where fronts have more time to accelerate, often experience stronger convective storms when triggered by sea-breeze effects.

1. Introduction

Gravity or density currents are predominantly horizontal flows where gravity drives fluid motion because of density gradients within a fluid. Such currents are ubiquitous in the atmospheric boundary layer (Smith and Reeder 1988). A common example is marine air advancing onto land as a sea breeze, which is initiated by differential solar heating of land and water surfaces (well-known examples include the Fremantle and Cape Doctors in Perth and Cape Town, respectively; Gentilli 1969). There have been numerous observational and numerical studies of sea breezes (Crossman and Horel 2010; Miller et al. 2003; and references therein) and high-resolution 3D large-eddy simulations (LES) that fully resolved boundary layer dynamical scales (e.g., Cunningham 2007; Fovel and Dailey 2001), though studies, such as (Robinson et al. 2011, hereafter RSG11) and Wu et al. (2009), have shown that 2D simulations can replicate important characteristics of observations.

* Supplemental information related to this paper is available at the Journals Online website: http://dx.doi.org/10.1175/JAS-D-12-0113.s1.

Corresponding author address: F. J. Robinson, Department of Geology and Geophysics, Kline Geology Laboratory, P.O. Box 208109, Yale University, New Haven, CT 06520-8109.
E-mail: frank.robinson@yale.edu

DOI: 10.1175/JAS-D-12-0113.1

As well as transporting cool marine air onshore, sea breezes can trigger cumulus cloud formation along the front of the advancing current. Deep convection observed over the Florida peninsula (Kingsmill 1995) and the Tiwi Islands (Chemel et al. 2009) occurs when either sea-breeze fronts (SBF) from opposite coastlines collide or SBFs collide with gust fronts somewhere over the land surface (Carbone et al. 2000). It has been suggested that this is due to a strong localized uplift caused by the displacement of fluid by the propagating sea breeze (Fovel 2005). The timing and location of deep convection triggered in this manner, both onshore and offshore, would then be controlled by the propagation speed of sea-breeze currents (e.g., Moncrieff and Liu 1999). A full understanding of the dynamics of density currents/sea breezes would therefore seem to be important for predicting the timing and severity of deep convective events; for example, cumulus parameterizations in GCMs are beginning to explicitly include cold-pool lifting effects, though with relatively little attention to their dynamics (Grandpeix and Lafore 2010).

An interesting aspect of sea-breeze dynamics is the sensitivity of sea-breeze convergence and subsequent ascent velocity to island width (Savijarvi and Matthews 2004). The optimal width (for strongest ascent) is not well defined and appears to depend on the type of heating, background stratification, and possibly other factors. Studies reported optimal scales ranging from 30–50 km (Abe and Yoshida 1982) to 100–150 km (Mahrer and Segal 1985; Xian and Pielke 1991). More recently, Robinson et al. (2008, hereafter RSL08) argued that deep convection in the atmosphere is particularly strong when the atmosphere is heated at the appropriate time and spatial scales to excite a ''resonance'' with respect to the propagation of internal gravity waves. Under these conditions the atmosphere has an equivalent depth set by the thickness of the near-neutral daytime boundary layer (about 1–2 km) and stratification of the morning sounding. They found that this mechanism could also explain the notoriously strong convection over the Tiwi Islands. Their theory essentially ignores density currents or any other form of horizontal advection, though density currents occurred in their simulations. The linear sea-breeze model employed by Rotunno (1983), which also ignores density currents per se, is very similar to the one used by RSL08 to explain deep convective intensity. Subsequent work by RSG11 found that that mesoscale dynamics driven by surface heterogeneity could explain the observed enhancement of convective strength over continents compared to oceans. While this study rejected common alternative hypotheses that the continental intensification was due to differences in humidity, boundary layer thickness, or aerosols, it did not further test the wave-dynamical mechanism proposed earlier. Given the apparent importance of density currents—which are highly nonlinear and are not fundamentally waves—it seems rather surprising that linear models have succeeded in simulating aspects of the sea breeze.

This enigma motivates a deeper understanding of the dynamics of density currents—in particular, whether they might have wavelike characteristics or somehow mimic (even if fortuitously) the behavior of gravity waves. In particular, the potential roles of environmental stratification and continuous solar forcing of the surface, which are crucial to wave theories, have not been carefully examined in studies of density currents. Indeed, previous observational and numerical simulation studies of sea-breeze and other density currents have typically compared their behavior to that of very simple laboratory analogs not considering either of these two effects, and have often found discrepancies (Crossman and Horel 2010).

The most well-studied theoretical and laboratory analogs for density current flows are the lock release and lock exchange. Dimensional reasoning and basic integral models have been used to predict the flow speed as a function of the initial conditions (see, e.g., Hogg et al. 2005; Huppert and Simpson 1980); however, the vast majority of research into density currents is based on the pioneering work of von Kármán (1940), Keulegan (1958), and Benjamin (1968). These models and subsequent developments (Rottman and Simpson 1983; Shin et al. 2004) make the assumptions that the flow is hydrostatic and steady, thus neglecting vertical accelerations. Further to these works on uniform density fluids, the effects of a stratified ambient fluid have been modeled both numerically and in the laboratory (for lock-release flows). Maxworthy et al. (2002) observed a complex interaction of current and waves and identified super and subcritical flows (where the waves where either trapped at the head of the current or propagated more quickly than the current and escaped periodically).

A stratified sea breeze will generally propagate into a daytime boundary layer that has already been well mixed by shallow convection—that is, an unstratified (or weakly stratified) layer capped by a more strongly stratified one, sometimes with an inversion at this interface (the opposite situation to that examined by Maxworthy et al. 2002). Haase and Smith (1989) and Liu and Moncrieff (2000) considered the case of a current with a constant stratification flowing into ambients with a range of stratifications, but did not examine the effect of varying the stratification of the current itself. The above studies have ignored two factors that we suggest may be important in the propagation of sea breezes—namely, stratification and continuous heating of the density current [though, recently, Seigel and van den Heever (2012) did look at the effect of the current stratification on cold-pool propagation].

Once stratification is present, waves become possible, and indeed it can become ambiguous whether propagating phenomena are more properly regarded as density currents or waves; Haertel et al. (2001) proposed that the fundamental distinction should be based on the relative importance of vertical versus horizontal advection of buoyancy, while in Mori and Niino (2002) the demarcation was stratification. One anticipates that wavelike dynamics will alter the behavior of the density current.

Another complication is that sea breezes on land ride over a surface that is continuously heated by the sun until evening. Many prior dynamical studies have considered only cases where a dense air mass is initiated somehow and there are no further buoyancy sources (Droegemeier and Wilhelmson 1987; Sha and Kawamura 1991). The sea-breeze simulations by Xian and Pielke (1991) included a diurnal cycle, but had an unrealistic initial condition that caused a rapid adjustment to steady state and consequently an approximately constant current speed. These idealizations may be reasonable for a thunderstorm outflow if the sky is very cloudy and insolation is weak, but would not apply to a sea breeze, which is driven by solar heating and develops in tandem with continuous heating. Indeed, Carbone et al. (2000) noted that certain sea-breeze fronts did not actually look like density currents, having smaller front speeds and Froude numbers than expected for a Benjamin-type density current, noting this as a possible cause.

Midlatitude and subtropical cold fronts resemble density currents near the frontal position, with the front location propagating relative to the background wind field and a low-level, relative flow into the front from the cold side, as found in a classical density current. Such fronts often obey the current speed equation even though the model underlying the equation does not appear applicable in general (Smith and Reeder 1988). Indeed, such systems are complex and are dominated by rotation (i.e., geostrophic), whereas the successful results noted earlier by RSG11 were obtained without rotation (and apply to tropical and subtropical storms). Surface heating has been found in models to significantly affect the behavior of fronts as they come onshore from the ocean (Reeder 1986; Thomsen et al. 2008).

In this study we analyze the ability of idealized density current theory to explain the behavior of sea breezes developing in the simplest possible realistic situations modeled by RSG11 and found to reproduce observed trends—namely, over simple heated islands with no topography or surface roughness, in two dimensions, and with no rotation. We focus in particular on the effects of ongoing surface heating and background stratification. We proceed by considering a progression of situations beginning with simple lock-release cases, adding first stratification, then steady heating, and finally diurnally varying heating.

2. Numerical simulations

a. Model description

All of the numerical simulations are done using the National Center for Atmospheric Research (NCAR)'s Weather Research and Forecasting (WRF) model version 3.0 (Skamarock et al. 2008), which solves the fully compressible hydrodynamic (Navier–Stokes) equations (Wicker and Skamarock 2002). It uses a third-order accurate Runga–Kutta scheme for the time integration, and second- to sixth-order accurate spatial discretization is available for the advection terms. The model supports closed periodic or open lateral boundaries and variable vertical grid spacing. The top boundary is a rigid lid and the bottom free slip. Note the use of a no-slip boundary condition in 2D can sometimes lead to trapped buoyant fluid at the base. This is because in 2D there is no physical method for this flow to escape, while in 3D it leads to the lobe and cleft instability.

For most of the simulations, the computational domain is 300 km in the horizontal and 25 km in the vertical, with open and rigid boundaries, respectively (for 100-km islands, tests were also made on a 500-km domain and it was found that the general trends were the same, while for larger islands a 500-km domain was always used). To minimize reflection of gravity waves by the upper lid, Rayleigh damping (sponge layer) is applied in the uppermost 5 km, with free-slip upper and lower boundaries. The horizontal and nonuniform vertical grid spacings are 125 and 25–100 m, respectively (at these resolutions no planetary boundary layer scheme was required). These simulations can be classified as 2D large-eddy simulations; the only parameterization used in the runs is 1.5 turbulent kinetic energy (TKE) closure scheme (Soong and Ogura 1980), which is used to model the subgrid-scale motions. Note as 2D fronts lack some of the energy-dissipating turbulent cascade, their turbulence characteristics are quite different from their 3D counterpart (Rotunno et al. 2011). However, as the results in this paper do not depend on turbulence effects, it is not a significant effect in the current study. We initialized the model with a mean temperature sounding from the station at Melville Island (11°33′S, 130°56′E) in northern Australia—a deep tropical site (see Fig. 1. of RSG11), but with water vapor and wind values set to zero.

b. Experiment design

Here we briefly describe the three types of experiments undertaken. These types progress from the simplest possible model in stages of increasing complexity in order to better understand the dynamics of cold-air outflows and sea breezes.

1) Lock release

The first and simplest simulations are an approximation of the classical dam-break or lock-release laboratory experiments in which a homogeneous cold fluid is released into a warm ambient. The initial potential temperature θ profiles offshore and over the land are shown in Fig. 1 (for three stratifications). One difference between these numerical configurations and the usual laboratory setup is that we include an overlying stable stratification (starting at a height of 1.6 km in this case). This is closer to an atmosphere that typically might have a mixed boundary layer capped by strong temperature stratification rather than an immediate jump to near-zero density at a liquid's free surface. Figure 2 shows contours of θ and horizontal velocity u in the x–z plane at different times after the release of the cold fluid (purple) into the warm ambient. In this and all subsequent contour plots, the unheated surface between −50 and 0 km is ocean and the heated surface between 0 and 50 km is land. As the left and right half of the ocean–island–ocean configuration are mirror images, we only show the left-hand side (i.e., the fronts always merge at 50 km east of the coast).

In this particular case the initial depth of the cold intrusion D is less than that of the mixed layer H, and it is called a partial-depth lock release. If $H = D$ then it is called a full-depth lock release. The values of H and D are marked on the first panel. The bounding black rectangle in the first panel marks the original location of the cold intrusion (which in this case is 1.2 K cooler than the warm ambient). Once the lock is released the cold fluid near the ground (purple) moves to the right at an approximately constant speed (see Hovmöller plots later in paper).

While H and D are specified at the start of the experiments, the current depth h is computed once the density current is in motion and is always defined as the mean height at which the flow velocity u within the density current is zero (level of return flow). The depth h is averaged over 12.5 km (100 grid points) from the current head back into the current and over one hour. The location of level h (also known as the thermal internal boundary layer or TIBL) is shown in the second and third contour plots of u.

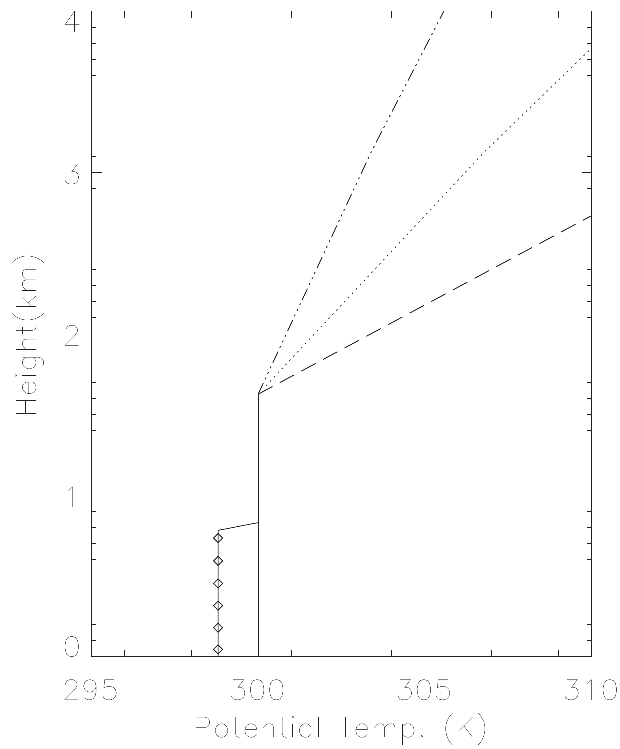

FIG. 1. Sample initial soundings for lock-release experiments, showing a partial-depth lock release where $D = 0.8$ km and $H = 1.6$ km (see Fig. 2), with three different values of upper-layer stratification S. The solid lines show the temperature profiles below H, which do not vary with S, with diamonds marking the profile in the cooler (ocean) region where it differs from that in the warmer (land) one. The triple dotted–dashed, dotted, and long-dash lines show the temperature above H for stratifications of 0.5 ×, 1 ×, and 2 × S_o, respectively.

2) Impulse heating

Sea breezes are typically made up of cold, stratified maritime air that penetrates a relatively well-mixed layer of warmer air over the land, which forms because of daytime surface heating and shallow convection. The potential temperature over the land approximately matches that of maritime air near the inversion, but is significantly higher near the surface. This situation is seldom considered in idealized and laboratory studies compared to the more common case where a homogeneous cold current penetrates a (possibly stratified) ambient—a setup that might be relevant to gust front outflows but not generally appropriate for sea breezes. Some numerical studies have, however, considered density currents with realistic internal stratification (e.g., Liu and Moncrieff 2000; Seigel and van den Heever 2012).

As a first step toward a more realistic sea-breeze front, we initiated ''impulse'' simulations with a large,

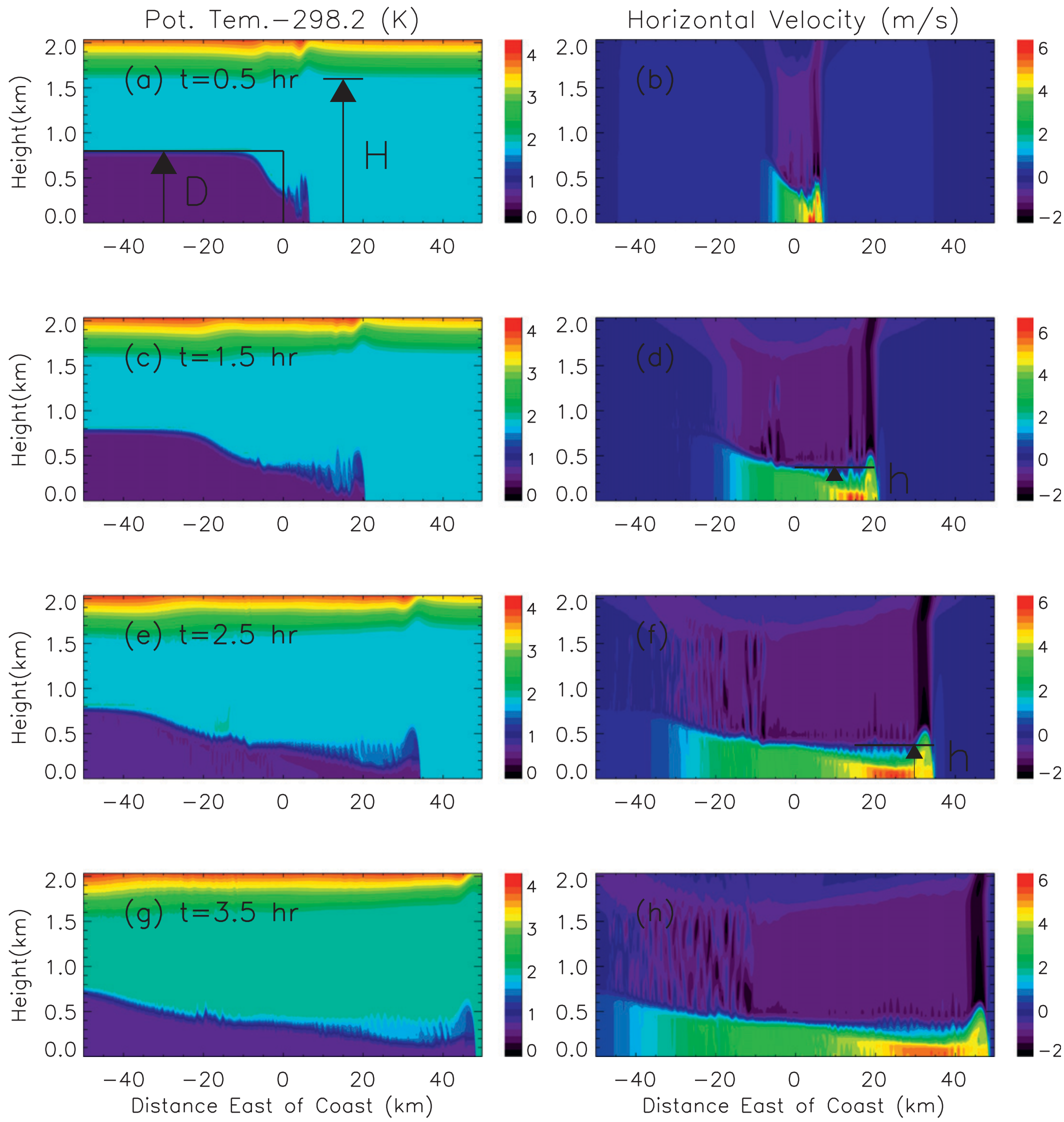

FIG. 2. Vertical cross section of (a),(c),(e),(g) potential temperature and (b),(d),(f),(h) horizontal velocity at (top to bottom) t = 0.5, 1.5, 2.5, and 3.5 h for a partial-depth lock release capped by a strongly stratified layer (case 12 in Table 1). In these and subsequent contour plots, the unheated region (ocean) is on the left half (−50–0 km) and the heated region (land) is on the right (0–50 km). The center of the island is at 50 km.

instantaneous surface heat input over the central 100-km ''land'' part of the domain. This heat input briefly produces unrealistically high surface temperatures, followed by intense turbulence that quickly creates a daytime mixed layer over the land. The temperature profile so created closely resembles that which would result from a gentler and more realistic input of heat from the sun, but by introducing it rapidly compared to the time scale over which a sea breeze can develop we approximately reproduce the situation common to more idealized studies where all potential energy is established by the (quasi-) initial condition, the current quickly attains a constant speed, and the flow is quasi conservative during the experiment.

Some representative, near-initial θ profiles are shown in Fig. 3. The heat input causes a near neutrally stratified boundary layer (of height H in the figure) to form within about 30 min, which is about 10% of the duration of the sea breeze, thus approximating the initial density contrast of classical lock-release experiments. These runs will be called impulse simulations. The main differences between these and the lock-release configuration are the stratification of the cold (offshore) fluid and the presence of residual turbulence in the warm boundary layer.

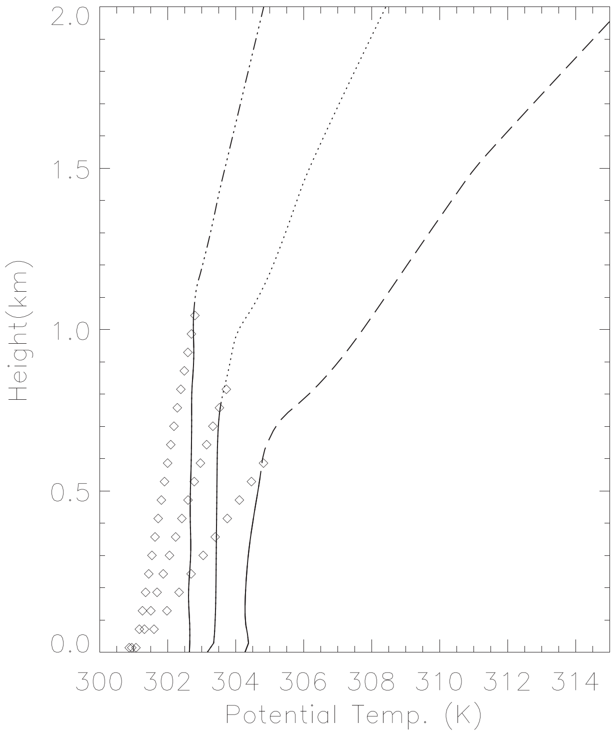

FIG. 3. Near-initial temperature profiles for impulse heating experiments with three values of stratification 30 min after application of the heating impulse. Below H, profiles differ significantly between the heated (land) and unheated (ocean) regions, with the latter's denoted by diamonds. Above H, profiles are approximately the same in either region, but vary according to S; profiles are shown for S of $0.5\times$, $1\times$, and $2\times S_o$, (cases 8, 9, and 10 in Table 2) with triple dotted–dashed, dotted, and long-dashed lines, respectively. Note the offshore S_o sounding is also the one used for all the continuous-heating runs.

3) CONTINUOUS HEATING

The final step in our hierarchy is to examine the implications of the fact that, in nature, heat is put continuously into the system gradually rather than all at once (although the impulse case may be relevant to cold-air outflows from thunderstorms). To examine the changes that result from ongoing heating at the surface, after the current has begun, we ran two sets of simulations with a ''top hat'' surface heat flux over the central 100 km (or 200 km to represent a larger island) of the domain but a horizontally homogeneous initial state (e.g., sunrise). The initial sounding for these cases is the same as the offshore sounding in the impulse runs with $S = S_o$.

In the first set, termed steady heating, we specified this at a constant heat flux $\dot{Q}_o$ of either 100 or 200 W m^{-2} (maintained for 6 h), while in the second, diurnally heated, we set the flux to be $\dot{Q} = \dot{Q}_o \sin(2\pi t/T)$ where $\dot{Q}_o$ is now the maximum flux (either 100, 200, or 400 W m^{-2}) and T is 24 h. (A constant heat flux of 100 W m^{-2} would add 1 MJ m^{-2} of energy every 2 ¾ h.) Figure 4 shows the accumulated heat for a steady and diurnally heated island both with $\dot{Q}_o = 200$ W m^{-2}.

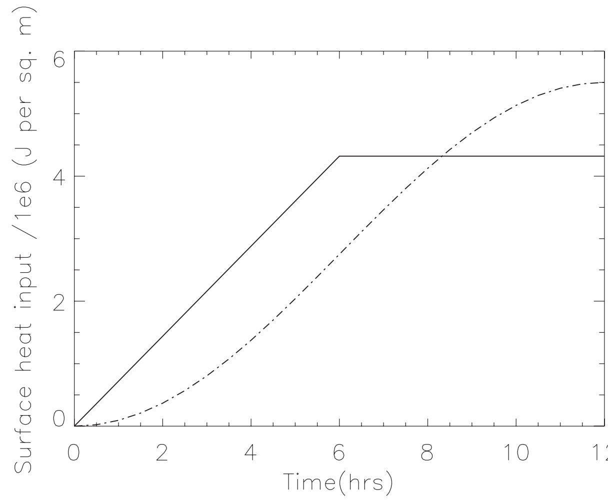

FIG. 4. Accumulated surface heat input vs time for steady (solid line) and diurnal (dotted–dashed line) heated with $\dot{Q}_o = 200$ W m^{-2}.

The diurnally forced case is more realistic, but the steadily forced case is easier to analyze. The behavior of the two, described in the next section, is relatively similar to one another compared to their stark departures from the impulse and lock-release cases.

3. Results

a. Lock release

We performed 12 lock-release-type experiments with initial horizontal temperature differences $\Delta\theta$ equal to 0.15 K up to 1.2 K and upper-level stratifications (above H) $d\theta/dz$ ranging through four octaves. Key prescribed quantities and results for the full- and partial-depth lock-release cases are presented in Table 1. Column 1 is the case identifier and column 2 is the ratio of the stratification above H to the control stratification S_o. The next columns in the table are H, D/H, the initial horizontal temperature difference $\Delta\theta = \theta_2 - \theta_1$ (where θ_1 and θ_2 are the initial temperature of the cold intrusion and warm homogeneous layer), the reduced gravity $g' = g\Delta\theta/\theta_2$, and a predicted Froude number

$$F_{\mathrm{HS}} = \frac{1}{2}\sqrt{\frac{D}{H}\left(2 - \frac{D}{H}\right)}, \qquad (1)$$

which is from Eq. (5.21) from Shin et al. (2004).

The remaining columns are h/H; the current speed, U; two Benjamin-type Froude numbers

TABLE 1. Characteristics of full- and partial-depth lock-release experiments with prescribed quantities given in columns 2–7 and those computed from the density current in columns 8–12. The stratification above H is denoted $S = d\theta/dz$; control stratification $= S_o$ is from a dry tropical sounding (see section 3a for definitions of the various Froude numbers).

Case	S/S_o	H (km)	D/H	$\Delta\theta$ (K)	g' (m s^{-2})	F_{HS}	h/H	U (m s^{-1})	F_H	F_h	$U/\sqrt{Q \times 10^{-5}}$ (kg^{-1})
1	1/8	1.6	1	0.3	0.01	0.50	0.44	2.5	0.63	0.94	1.1
2	1/4	1.6	1	0.3	0.01	0.50	0.43	2.3	0.58	0.88	1.1
3	1/2	1.6	1	0.3	0.01	0.50	0.42	2.2	0.55	0.85	1.0
4	1	1.6	1	0.3	0.01	0.50	0.44	2.2	0.55	0.83	1.0
5	1	0.8	1	0.3	0.01	0.50	0.41	1.7	0.60	0.94	1.1
6	1	3.2	1	0.3	0.01	0.50	0.40	2.9	0.50	0.81	0.9
7	1	1.6	1/8	0.3	0.01	0.24	0.08	1.2	0.30	1.10	1.6
8	1	1.6	1/4	0.3	0.01	0.33	0.13	1.5	0.38	1.10	1.4
9	1	1.6	1/2	0.3	0.01	0.43	0.25	1.9	0.48	0.95	1.2
10	1	1.6	1/2	0.15	0.005	0.43	0.27	1.3	0.46	0.88	1.2
11	1	1.6	1/2	0.6	0.02	0.43	0.24	2.6	0.46	0.94	1.2
12	1	1.6	1/2	1.2	0.04	0.43	0.27	3.8	0.48	0.91	1.2

$$F_H = U/\sqrt{g'H} \quad \text{and} \tag{2}$$

$$F_h = U/\sqrt{g'h}; \tag{3}$$

and finally the ratio of U to $\sqrt{Q \times 10^{-5}}$, where Q is the heat deficit of the cold intrusion, $Q = \rho c_p \Delta\theta D$, and c_p and ρ are the specific heat capacity and density of dry air.

In most cases F_h is close to unity, in approximate agreement with Fig. 7 of Benjamin (1968) (with h/H and F_h as the x and y axes in the current notation), though it decreases slightly with upper-layer stratification. In these experiments the release of energy is typically quite abrupt with the flow becoming steady almost immediately after the lock is released. The stratification effects are relatively modest for the present purposes, but interesting. The U reduces from 2.5 to 2.2 m s^{-1} as the stratification of upper layer is increased (cases 1–4 in Table 1) [in agreement with Liu and Moncrieff (2000)]. This is because as the current travels along it has to push fluid out of its way, and a standing wave between the head of the current and the top of the mixed layer is formed. This can be seen in Fig. 2 as a bump at the inversion directly above the head of the current (at the top of each of the θ figures). This interfacial wave then perturbs the potential temperature surfaces generating gravity wave propagation. For the control case (row 4), the turbulent kinetic energy per unit mass in the gravity waves, $1/2[(u')^2 + (w')^2]$, is about 10% of the current kinetic energy per unit mass, $(1/2)U^2$ (here $u' = u - \langle u \rangle$, where $\langle u \rangle$ is the horizontal average.) This phenomenon will be studied further in a subsequent article.

As these losses of energy are modest, at least in these examples, for a given intrusion depth D the current speed appears to be very well determined by either Benjamin formula [Eq. (2) or (3)] or the initial equivalent (negative) heat input per unit domain area Q required to create the actual initial condition from a horizontally uniform prototype. For example, when $\Delta\theta$ is increased from 0.15 to 0.6 K, U also doubles, so the kinetic energy of the current goes up by a factor of 4 (e.g., compare cases 10 and 11). The latter result is hardly surprising since the equivalent heat input is proportional to Hg', which is precisely the term in F_H. However, it will be of greater interest in analyzing subsequent cases.

Neither the Benjamin formula F_H nor the initial energy Q fully explains the changes for partial-depth lock experiments (e.g., when D/H becomes smaller than one). In these cases the current does not slow down as much as would be predicted with invariant h/D and F_H (less than $\pm$10% change). The values are, however, quite close to those predicted by Ungarish (2009). For example, Fig. 5.11 of Ungarish (2009) presents graphs of equivalent quantities to h/D and $U/\sqrt{g'D}$ that are consistent with cases 4, 7, 8, and 9 in Table 1 (e.g., for $D/H = 1$, ½, ¼, and ⅛ we find $h/D = 0.5, 0.5, 0.5$, and 0.6 and $U/\sqrt{g'D} = 0.4, 0.5, 0.7$, and 0.8). The Shin et al. (2004) formula comes close to predicting the observed halving of the Froude number (though F_{HS} is consistently about 10% smaller than the measured values of F_H). This indicates that to understand these partial-depth lock results may require an analysis such as Shin et al. (2004) or Ungarish (2009) rather than simple energy metrics.

b. Impulse heating

We performed 15 impulse experiments of 100-km-wide islands with background stratifications $d\theta/dz$ ranging through four octaves and surface heat inputs Q ranging from 0.5 to 2.0 MJ m^{-2}; experiment parameters and key results are listed in Table 2. For these runs, since we no longer have two initial fluids of constant θ, we estimate H (see Fig. 3) and g' from the transient part of the flow as $g' = g(\theta_{\text{int}} - \theta_{\text{cur}})/\theta_{\text{int}}$, where θ_{int} is the potential

TABLE 2. Characteristics of impulse heating experiments with prescribed quantities given in columns 2 and 3 and those computed from the density current in columns 4–10. Stratification $S = d\theta/dz$; control stratification = S_o is from a dry tropical sounding. Other symbols described in text.

Case	S/S_o	$Q/10^5$ (J)	H (km)	h/H	U (m s^{-1})	g' (m s^{-2})	F_H	F_h	$U/\sqrt{Q \times 10^{-5}}$ (kg^{-1})
1	1/8	5	1.7	0.42	1.9	0.005	0.64	1.0	0.85
2	1/4	5	1.2	0.39	1.9	0.009	0.57	0.9	0.85
3	1/2	5	0.9	0.34	1.9	0.015	0.53	0.9	0.85
4	1	5	0.6	0.33	2.0	0.020	0.60	1.1	0.89
5	2	5	0.35	0.32	2.0	0.030	0.62	1.1	0.89
6	1/8	10	2.5	0.41	2.6	0.008	0.58	0.9	0.82
7	1/4	10	1.9	0.35	2.6	0.013	0.53	0.9	0.82
8	1/2	10	1.2	0.36	2.8	0.017	0.62	1.0	0.89
9	1	10	0.9	0.31	2.9	0.027	0.58	1.1	0.91
10	2	10	0.6	0.30	2.9	0.038	0.63	1.1	0.91
11	1/8	20	3.1	0.41	3.7	0.013	0.58	0.9	0.83
12	1/4	20	2.6	0.38	3.6	0.019	0.52	0.8	0.80
13	1/2	20	1.8	0.38	3.6	0.028	0.50	0.8	0.80
14	1	20	1.3	0.36	4.0	0.037	0.58	1.0	0.89
15	2	20	0.9	0.30	4.0	0.060	0.56	1.0	0.89

temperature of the interior fluid (sampled at the center of the island; i.e., at $x = 50$ km) averaged vertically over 0 to h, and θ_{cur} is the potential temperature of the current averaged horizontally (over the first 12.5 km behind the current head) and vertically (between 0 and h). Quantities g', h, and H have also been averaged over the time between the formation of a well-defined current (30 min) and the merge of the opposing fronts (which occurs typically between 3 and 4 h).

As in the lock-release case, the cold current again propagates inward at a constant speed for each of the 15 runs. For a given stratification this speed varies from 2 to 4 m s^{-1}, and is only a function of heat input. The left column of Fig. 5 shows the potential temperature, velocity, and pressure perturbation (contoured and presented at three different heights) for the control stratification S_o (case 9 in Table 2). The current formed in this impulse case has a similar head shape to that in a partial-depth lock release (e.g., compare Fig. 2c and Fig. 5a) with the current-locked internal wave train seen as the small bump in the mixed layer directly above the current head (located approximately at $x = 20$ km, height = 2 km in Fig. 5a).

The current speed is again modestly affected by stratification, in this case increasing by 5%–10% going from the weakest to strongest stratification for a given heat input [in agreement with Seigel and van den Heever (2012)]. This appears to be mediated partly by mixing between the oppositely moving currents, but this will be further investigated in subsequent work. As stratification increases, both the boundary layer depth H and current thickness h decrease, but the density contrast g' strengthens exerting a compensating effect on the current speed.

The decreases in h with stratification are slightly greater than those of H, but their ratio varies by no more than 30%, even though H changes by an order of magnitude (the extremes being cases 5 and 11). Thus, to a reasonable approximation the thickness of the density current appears to be determined by that of the mixed layer over land and is about 1/3 of the latter.

The Benjamin formula holds within about ±10% if referred to the actual intrusion height h, with values of F_h ranging from 0.9 to 1.1 in most cases, although a couple of the weakly stratified and strongly heated runs fall to 0.8. This is a remarkably consistent Froude number given that g' varies by a factor of 10. The Froude number calculated with respect to H is similarly consistent, and clusters around 0.55.

Another remarkable result is that the kinetic energy of the current per unit mass U^2 is very nearly proportional to the energy input Q across all parameter variations, to an even greater degree than for the lock-release simulations. The result is more interesting here as it holds despite large changes in the internal stratification of the currents, which profoundly affect their character. This result is consistent with the scaling given in Antonelli and Rotunno (2007), who further show that $H \propto \sqrt{Q/N}$. We can confirm that the variation with N also holds here by comparing two runs with the same Q but different S/S_o, such as cases 2 and 4. Here the stratification is quadrupled, but H is halved ($N \propto \sqrt{S}$). The ratio $U/\sqrt{Q}$ is about 10% smaller than that of the full lock experiments, implying that these currents are traveling about 10% more slowly for the same initial energy input than did the full lock ones.

c. *Continuous heating*

A snapshot of a typical current is shown in Figs. 5e–h. A notable difference from the impulse case (Fig. 5a

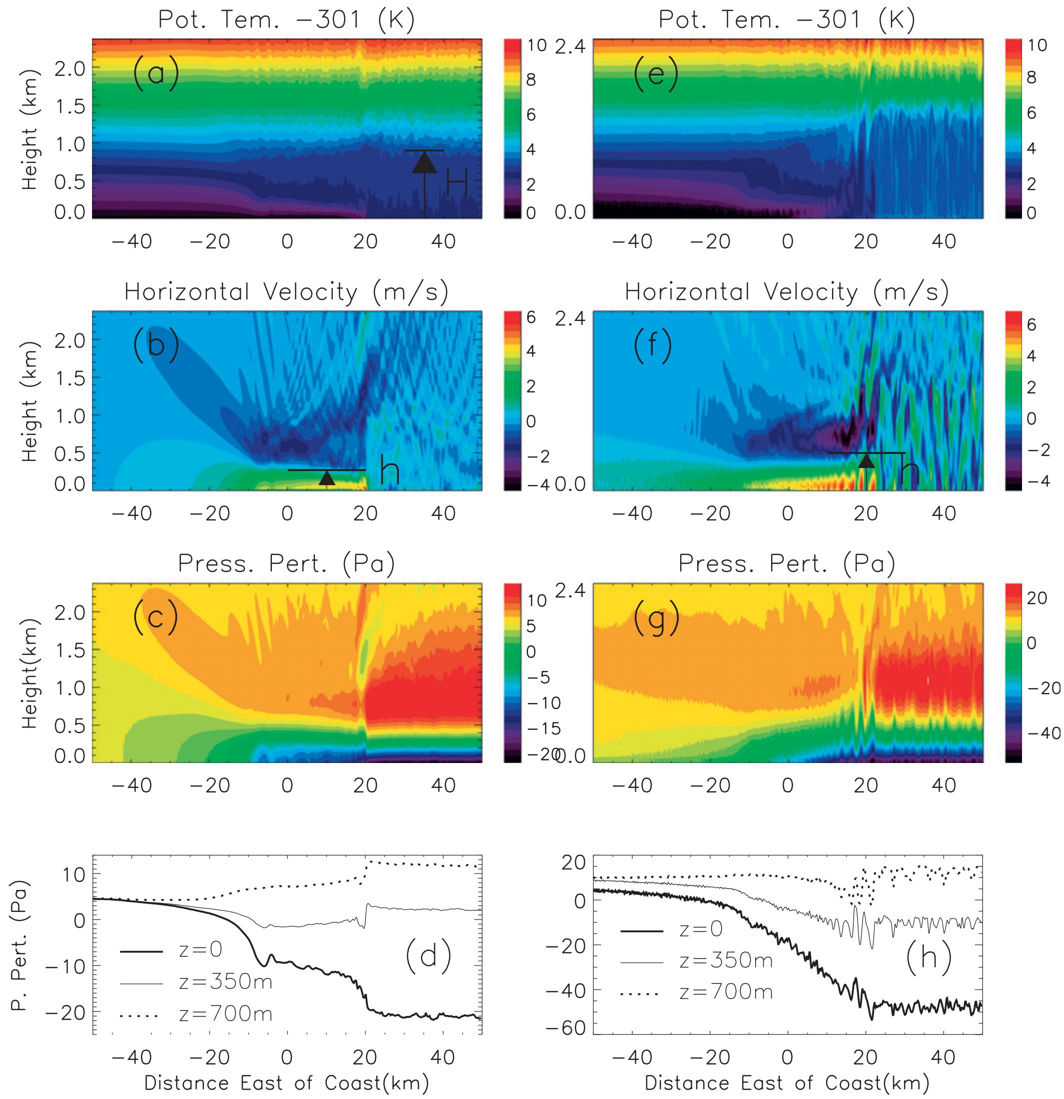

FIG. 5. Vertical cross section of (a),(e) potential temperature, (b),(f) horizontal velocity, (c),(g) pressure perturbation, and (d),(h) pressure perturbation at the surface and at $z = 350$ and 700 m, for (a)–(d) an impulse case at 2 h (case 9 in Table 2) and (e)–(h) the steady heating case at 6 h with $\dot{Q}_o = 100$ W m^{-2}.

versus Fig. 5e) is that the potential temperature within the current increases steadily as one approaches the head (located near the surface at $x = 20$ and 22 km in Figs. 5a and e, respectively), by which time it has become almost equal to that ahead of the current—in other words there is little density contrast across the head of the current. The velocity distribution on the other hand continues to show a sharp front in both cases (Fig. 5b versus Fig. 5f); thus, the head is still a sharp and well-defined feature, temperature field notwithstanding. Similarly, the pressure perturbation (Fig. 5c versus Fig. 5g), defined as the difference between the pressure at time t and at $t = 0$, drops sharply by about 10 Pa near the ground at $x = 20$ km in the impulse case, while in the continuously heated case there is a more gradual reduction of ~40 Pa between $x = -20$ and 20 km over the entire body of the density current. The difference in the horizontal pressure gradients between the two cases is easier to see if the pressure perturbation is plotted at specific heights (Fig. 5d versus Fig. 5h).

Several other qualitatively new features appear in the continuously heated cases. First and most importantly, the current velocity is no longer constant. The evolution in time of θ and u with horizontal distance from the coast is presented in the Hovmöller (HM) plots; see Fig. 6. These plots clearly show a constant front velocity for the lock and impulse cases (Figs. 6a and c) but acceleration for the continuously heated cases (Figs. 6e and g). In all

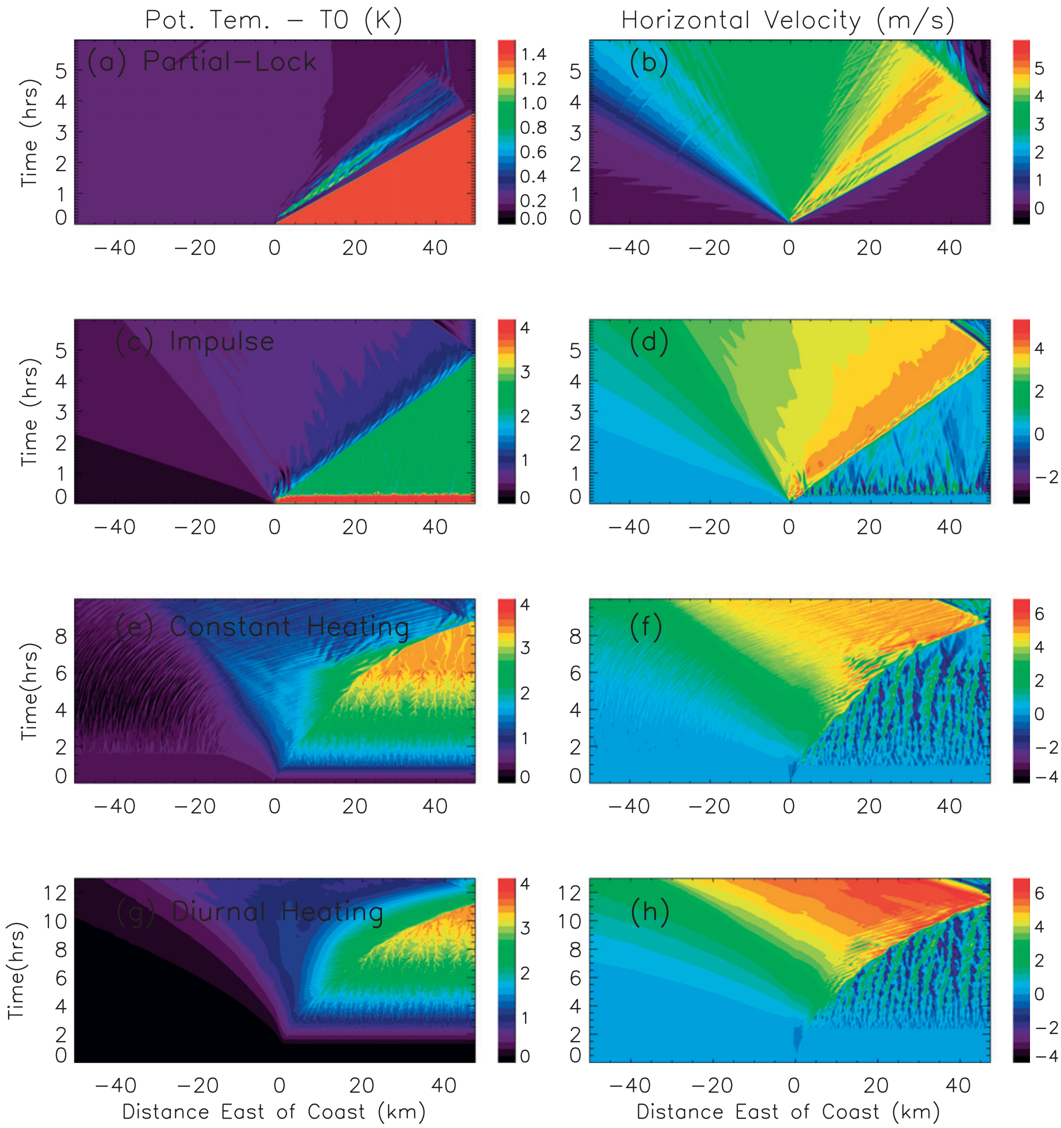

FIG. 6. Hovmöller plots of (a),(c),(e),(g) potential temperature minus T0 and (b),(d),(f),(h) horizontal velocity for (top to bottom) sample partial-depth lock release (case 12), impulse heating (case 9, $Q = 1 \times 10^6$ J and $S = S_o$), constant heating, and diurnal heating cases ($L_x = 100$ km and $\dot{Q}_o = 100$ W m^{-2}). The temperature offset T0 is 298.2 K for the partial lock release and 301 K for the impulse, constant heating, and diurnal cases. In each case, the heated surface or "land" is between 0 and 50 km east of the coast and variables are sampled at a height of 100 m above the surface.

cases the current head is a well-defined feature of the velocity field.

These plots also reveal the temperature gradient noted earlier within the current, visible as a bulge of green or light blue color above and to the left of the front position, absent in the impulse case. Additionally, the lock-release case shows the transient appearance of warm fluid as a multicolored filament in the graph; this is due to the entrainment of warm fluid down to low levels behind the current via Kelvin–Helmholtz instabilities as reported, for example, by Sha and Kawamura (1991), but does not affect the density contrast ahead of the current. Similar warming can be seen in the continuously heated cases but much farther downstream of the head, appearing as blue swaths extending up and to the left in regions of strong inward velocity; these features again appear to be due to downward mixing of high-theta air through the cold current, perhaps aided by the residual turbulence advected from the warm boundary layer (see the lower right of the figure panels). This mixing does not reach the 100-m level in the impulse case.

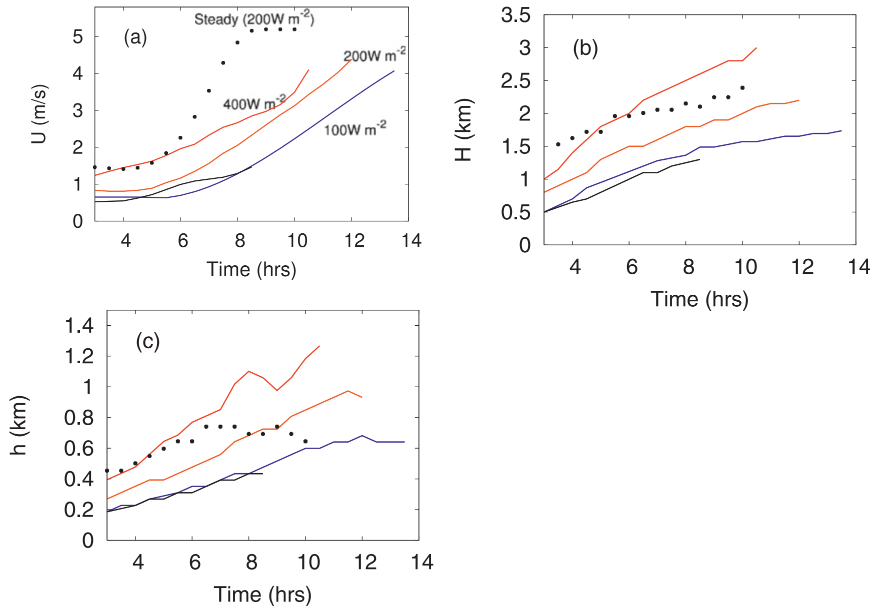

FIG. 7. Current data for five different island simulations with (a) U and (c) h computed near the head of the moving current (see main text) and H at the island center. The steady heating case with $\dot{Q}_o = 200$ W m^{-2} on a 200-km island is delineated by black symbols. The four other line plots are for diurnally heated islands; blue, orange, and red lines are 200-km islands with $\dot{Q}_o = 100, 200$, and 400 W m^{-2}, respectively, and the black solid line is for a 100-km island with $\dot{Q}_o = 100$ W m^{-2}. Quantities are plotted from the time a well-defined front has formed (e.g., see Figs. 6g and h) up to time of the merge of the opposing fronts.

d. Front position and current characteristics

To extract the front position from the HM plots we developed a simple Matlab algorithm as follows: a 2D gradient field of the potential temperature is generated for a given level (typically at 100 m). This data contains the position of the front (and in some cases erroneous data from the convecting plumes, etc.). The data is thresholded and the position of the remaining points extracted; the data is then manually checked and any

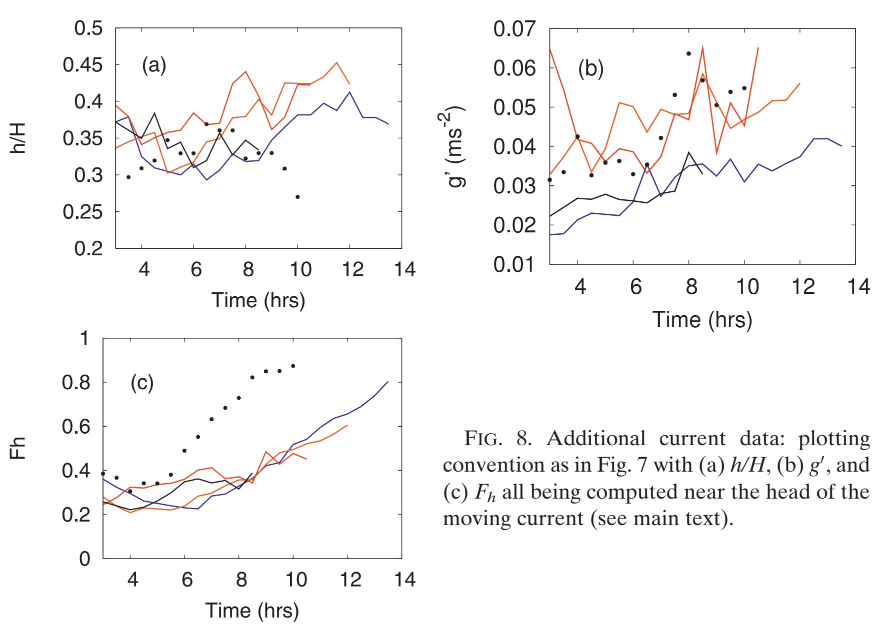

FIG. 8. Additional current data: plotting convention as in Fig. 7 with (a) h/H, (b) g', and (c) F_h all being computed near the head of the moving current (see main text).

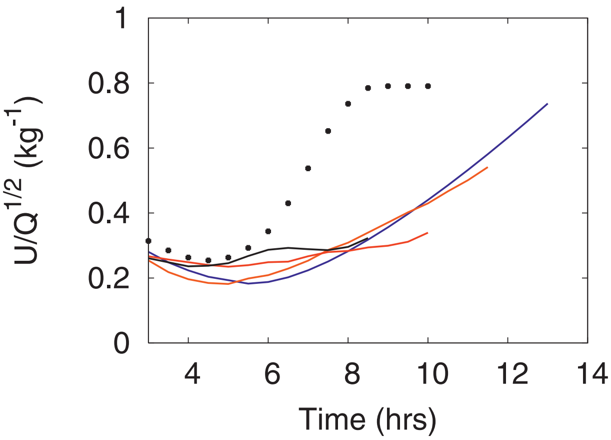

FIG. 9. Ratio of front speed to square root of surface heat input: plotting convention as in Fig. 7.

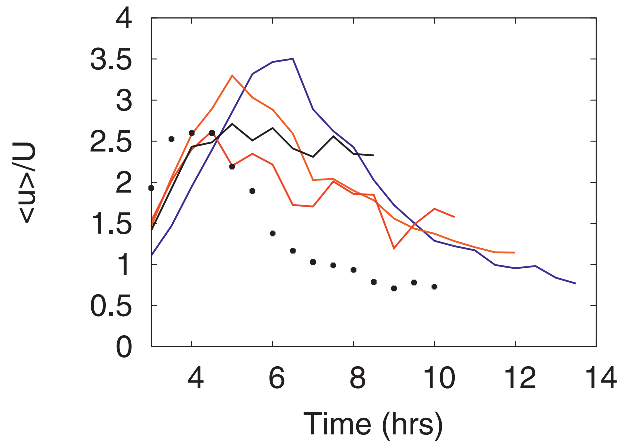

FIG. 10. Ratio of the mean horizontal flow speed inside the current head $\langle u \rangle$ to the front speed U: plotting convention as in Fig. 7.

spurious data is removed. Finally, the remaining points have a least squares curve fitting algorithm applied to generate a polynomial best fit.

The time variation of quantities describing the density current is shown in Figs. 7–8 for a 200-km steadily heated island, three diurnally heated 200-km islands, and a 100-km diurnally heated island. This reveals a significantly more complicated picture than in the previous cases. The steadily heated island having $\dot{Q}_o = 200$ W m^{-2} is denoted by filled black circles and the diurnally heated examples by solid lines. The colors represent different heating rates with $\dot{Q}_o = 100$ (blue), 200 (orange), and 400 W m^{-2} (red). To identify effects of island width, the results from a 100-km island diurnal run with $\dot{Q}_o = 100$ W m^{-2} is shown by the solid black line.

In each case after $\approx$(3–6) h the front velocity U (Fig. 7a) starts to increase approximately linearly in time, from small initial values to speeds comparable to or slightly slower than those seen in the impulse cases (for a similar energy input Q). For example, by 10 h the steady-heated case has accumulated more than 4 MJ and has a maximum speed of about 5.2 m s^{-1}, while according to Table 2 an impulse case with an input 4 MJ would have a front speed of about 5.6 m s^{-1}.

In the steady heated case, as the heat is turned off at 6 h (Fig. 4) it takes about two hours for the cold offshore air to catch up with front, after which the speed remains constant. Contributing to this are increases in H and h, each of which increases by a factor of 3 over the period retaining a ratio of roughly 3:1 across all simulations (Fig. 8a) while the density contrast g' roughly doubles (Fig. 8b).

However, these increases in h and g' are insufficient, according to Eq. (3), to explain a quadrupling or more of U found in the simulations. Indeed, F_h (Fig. 8c) increases from an initial low value of about 0.3 to about 0.5–0.8 (the maximum value depending on when the fronts collide at the center of the domain). Thus, Benjamin's formula for F_h, which predicts a value of 1.0 and was correct for the impulse case, fails badly for all the continuously heated cases. Moreover, the kinetic energy relationship that succeeded on the impulse case predicts, for our steady-heating case [where $Q = \dot{Q}_o t$ and $U \sim \sqrt{(Q)}$], that $U \sim \sqrt{(t)}$—when in fact we see something closer to $U \sim t$.

To see how the heat input Q is partitioned between the mean horizontal flow inside the current $\langle u \rangle$ and the bulk velocity of the front U, consider Figs. 9 and 10, which show the ratios $U/\sqrt{Q}$ (kg^{-1}) and $\langle u \rangle/U$ (each computed in the frame of reference of the moving current versus time). The quantity $\langle u \rangle$ is the horizontal velocity averaged over 0 to h and from the front to 10 km in from the front. For most of the time before the opposing fronts collide, $\langle u \rangle$ is 2–3 times faster U, so the kinetic energy of the current is typically about an order of magnitude greater than $(1/2)U^2$. Hence, for most of the duration, the majority of the kinetic energy appears as a flow inside the current, rather than in propagation of the front and current as a whole.

We are then faced with several questions: Why do Benjamin's formulas break down? Why does the temperature distribution change so much? And why does the current accelerate? We do not have a complete quantitative theory for this case, but provide below a preliminary diagnostic analysis helping to explain these phenomena.

4. Preliminary explanations of continuous-heating phenomena

a. Temperature

Among the new phenomena emerging with continuous heating, the easiest to explain is the temperature distribution. As the land continuously heats the air above, the cold current moving over it gradually heats up. This means that the temperature of the density current will increase with distance inland, significantly reducing g' compared to an impulse case with an initial Q equal to the accumulated Q in the continuously heated case (noting that in the impulse case all of the heat goes into the air ahead of the density current).

Quantitatively, the potential temperature near the ground should be governed approximately by

$$\frac{D\theta}{Dt} = \frac{Q}{c_p \rho H_{\text{mix}}}, \tag{4}$$

where D/Dt is the material derivative, Q is the surface heat flux, and H_{mix} is the depth through which the heat mixes or through which the mean of temperature is taken (we assume pressure is near the reference value, neglect both diffusion, the energy to heat soil surface and radiative heat sources). In the interior (ahead of the current), the bulk velocity is zero so that the material and local derivative are identical, and we take $H_{\text{mix}} = H$, the mixed layer height, so that the increase in temperature of the air in the interior over time Δt is

$$\Delta\theta_{\text{int}} \sim \frac{Q}{\rho c_p H}\Delta t. \tag{5}$$

In the density current the situation is more complicated. As the front moves across the land, the current head is constantly being fed with cooler air from the sea. As the land heats up, some of this cooler air will be heated as it is traveling over the land. To a first approximation (i.e., ignoring effects of entrainment and vertical velocity), the temperature of the air near the head of the current is determined by two competing processes: (i) heat from the ground $Q(t)$ and (ii) cool air being advected into the current head (which then overturns returning above the $u = 0$ surface).

Consider the head of the current with the $u = 0$ surface as a material surface. If the front moves a distance Δx (small enough that U and u are approximately constant) then the time the air in the current has felt heating from below is

$$t_h \sim \frac{\Delta x}{\langle u \rangle}, \tag{6}$$

where $\langle u \rangle$ is the mean horizontal speed of the air inside the current.

Over the distance Δx, the current is moving at speed U so that

$$\Delta x = U\Delta t, \tag{7}$$

where Δt is the time it takes for the current to move Δx.

Combining these two equations gives

$$t_h \sim (U/\langle u \rangle)\Delta t. \tag{8}$$

Hence, over the time interval Δt the change in the temperature of the head of the current due to heating from below will be

$$\Delta\theta_{\text{cur}} \sim \frac{Q}{\rho c_p h} \times (U/\langle u \rangle)\Delta t. \tag{9}$$

For reasons discussed shortly, the velocity $\langle u \rangle$ of the air inside the current in these simulations is several times faster than the propagation speed U of the front. This greater speed will advect cold sea air toward the front at a much faster rate than the propagation speed of the front itself, which means the air arriving at the front has had less time to pick up surface heating than has air ahead of the front. In other words, the ability of the land to warm up (low level) cool sea air traveling over it is reduced if $\langle u \rangle$ increases. So the faster the flow inside the current, the greater the temperature drop across the density current. This strengthens g', sharpening the density jump at the current head as observed (e.g., Thomsen et al. 2008), while feeding back negatively on the torque that created it.

For simplicity, if we neglect the time dependence of parameters, we can solve for the temperature difference across the front, obtaining

$$\theta_{\text{int}} - \theta_{\text{cur}} = \frac{Qt}{\rho c_p H}\left(1 - \frac{UH}{\langle u \rangle h}\right). \tag{10}$$

To keep this difference positive and the air behind the front cooler than air ahead of it, we must have $(\langle u \rangle h) > UH$. Since $H/h \approx 3$ robustly across all experiments and times, the inflow speed $\langle u \rangle$ must be at least 3 times the front speed. In the impulse cases, $\langle u \rangle/U \sim 1.2$; thus, the greater $\langle u \rangle/U$ found in the continuous-heating simulations appears to be essential to overcome the inhibitive effect of continuous heating. Moreover, Fig. 10 shows that $\langle u \rangle$ begins to accelerate before U (Fig. 7a) and that the maximum of $\langle u \rangle/U$ is near the required value of 3 when U actually starts to increase. This behavior is consistent with our reasoning that $\theta_{\text{int}} - \theta_{\text{cur}}$ needs to be positive to accelerate the current. Toward the end of the front propagation $\langle u \rangle/U$ approaches unity, which is close to the value found in the impulse case (note as $U = 0$ at $t = 0$, $\langle u \rangle/U$ is undefined before the sea breeze starts moving).

b. *Dynamics*

The acceleration of U just noted is attributable to the horizontal temperature gradient within the density current caused by the continuous heating. This gradient drives hydrostatically a torque within the inflow, hence generating vorticity within the moving current (via the baroclinic production term $\rho^{-2}\nabla\rho \times \nabla p$ in the vorticity equation). This speeds the inflow near the surface while slowing it in the top part of the current (this effect would presumably be damped without a free-slip lower surface, but we have not quantified this). This vorticity generation is most evident near the coast ($x = 0$), where u near the surface continues to increase with time after the departure of the front (Figs. 6f and h), in contrast to the impulse and lock-release cases where the velocity slightly decays with time (Figs. 6b and d). A symptom of this may be seen by comparing the pressure distributions for the impulse and continuous cases (Fig. 5c versus Fig. 5g and Fig. 5d versus Fig. 5h). Near the surface, there is a large pressure drop at the front (x = 20 km) in the impulse case with relatively weak gradients elsewhere; whereas in the heated case, there is a more uniform pressure gradient extending far behind the current head. Moreover, this pressure gradient extends much higher in the heated case, up to 700 m or so even though the $u = 0$ level is at 400–500 m and acts to decelerate the return flow. The movie of the potential temperature field over the left half of the 200-km island (that accompanies this article) clearly shows this return flow entraining fluid from ahead of the current back into the sea-breeze current.

In lock-release and impulse experiments, where the density contrast is set up in the initial condition, the two density currents move at velocities that remain approximately constant both in time and along the length of the current once they get started. This motion is essentially inertial. Vorticity in the flow is concentrated in the shear zone between the two currents. Net forces and accelerations are concentrated in the immediate vicinity of the fronts; fluid just ahead of the lower front is accelerated upward then rearward, making way for the advance of the current. These accelerations are driven by the pressure drop, determined by the temperature difference according to Eq. (3).

The success of the Benjamin formulas in these cases is not because of an instantaneous force balance at the current head as might be suggested by the term $g'h$—a hydrostatic pressure difference. It is rather because $\sqrt{g'h}$, no matter when it is measured, records the initial torque impulse that first propelled the two currents into motion. After this initial impulse, both the velocity and the product $g'h$ are constants of the motion for the special case of steady flows.

The acceleration of the front seen in the continuous-heating simulations, in particular, requires the continuous generation of additional vorticity all along the length of the currents near height h. This is provided by a landward pressure gradient extending from the ground to several hundred meters above the zero-motion level. The pressure gradient is probably associated with the vorticity generation by the horizontal temperature gradient near the surface, but involves a much larger volume of air. It appears to be nearly constant in time, resulting in a steady acceleration of U. Meanwhile, there is significant vorticity below the $u = 0$ level, which is being advected toward the head of the current. This can be clearly seen in the supplemental movie of the θ field for a continuously heated current case.

It should be clear from this discussion that changing the density contrast across the front cannot, on its own, lead to a change in velocity of the front as naively predicted from Benjamin's formulas. The front cannot simply run out ahead of the current. Indeed, the quantity g' is not well defined in the heated cases because temperature decreases with distance behind the front and is nearly constant across the front. For the system to accelerate as a whole, pressure gradients must be set up throughout the entire current. We believe this is the fundamental reason for the failure of the Benjamin formulas, and in particular, for the delayed acceleration of the current head and consequently low Froude numbers, in cases where the density contrasts are introduced gradually rather than as an initial condition. Further studies could attempt to model this more carefully with simplified flow models.

5. Discussion and conclusions

This study has produced two main results: one concerning the effects of stratification on density currents and one concerning the effects of ongoing surface heating on the current.

First, we find that in the case where a density contrast is created near instantaneously in stratified fluid by heating one part of the domain from below, the total energy input needed to do this is a surprisingly robust indicator of the speed of the resulting density current (Table 2). This is true for a very wide range of stability values and a range of total energy inputs, producing a range of current depths. The predictor works also for full lock-release cases (but not very well for "partial-depth lock release"). The speed predicted from this is more accurate ($\pm$5%) than could be diagnosed from the Benjamin formula based on the estimated parameters of the flow (h and g'), let alone from the known initial conditions. This scaling was predicted theoretically by Antonelli and Rotunno (2007). While this result is interesting, its practical utility is limited because the heating that would produce this situation would normally be gradual rather than near instantaneous; in that case, the limiting speed is attained only if the heating is switched off, and only well after the time that happens (in simulations here, several hours afterward).

Indeed, our second and more important result relates to what happens when cold-air inflows are generated more realistically by a steady input of heat from a continental surface, rather than an initially specified density contrast as typical in laboratory analogs and past idealized computations. Observations by Carbone et al. (2000) over the Tiwi Islands found F_h values of 0.5–0.6 and front speeds of 1–2 m s^{-1}, and speculated that the differences between ''dam break [theory] and sea-breeze was due to diabatic heating as air passes over a monotonically increasing fetch of land.'' We would concur with this explanation, and have presented simulations showing that indeed the presence of ongoing surface heating slows the current propagation.

Moreover, the longer acceleration times over larger islands could lead to stronger convection. Thus, the dynamics of sea-breeze fronts may in part explain the observed increase in convective vigor as a function of island size. However, since the dynamics of the transient accelerating sea breezes are not yet fully understood, it remains unclear whether the dispersion relation proposed by RSL08 is generally applicable, though the linear theory of sea breeze by Rotunno (1983) is a very similar model. Further study is clearly needed to resolve this enigma.

All currents simulated here show an internal circulation, with near-surface winds outrunning the front itself. Consequently, from mass conservation, the frontal boundary is taller than the current, by roughly a factor of 2 for steady currents (e.g., Fig. 2f). The main change associated with steady surface heating is the generation of internal temperature gradients and vorticity within the cold current, which cause a shallowing and intensification of the internal circulation while weakening the density contrast at the front itself, slowing the frontal propagation. Thus, the sea breeze arrives later but is followed by stronger near-surface winds.

Lock-release experiments have a very quick adjustment to a steady state so that most of the energy in the lock is given to the current and intrusion with about 10% being lost as wave energy. This energy loss occurs because the current head pushes on fluid in front of it and a standing wave forms between the current head and the top of the mixed layer (e.g., Fig. 2a), moderating the current speed. Conversely, in the more realistic situation of gradual heating over a day, the energy is partitioned over the entire current, resulting in a slowly increasing front speed. Because of this diurnal heating the Froude numbers characterizing real density current are initially much less than those given in the experiments and only approach theoretical values in the mature stage of a sea-breeze front.

If surface heating is switched off, currents eventually begin to resemble their impulsively generated counterparts through a process of frontogenesis whereby the accelerated near-surface winds advect cold air toward the head of the current. A similar mechanism was seen in Muir and Reeder (2010), though in their case there was also a background wind profile, so the dynamics are slightly different (they also included surface roughness effects, which we have not). This process, however, takes several hours in the cases examined here where heating was switched off at midday. Thus, real sea breezes do not come near the steady state condition assumed in idealized theories.

The propagation speeds of sea breeze and other mesoscale frontal phenomena affect daytime weather variations and will affect the timing of convective triggering in cases where this occurs. Other aspects of the dynamics illustrated here may also be important for the triggering of convection. For example, heating of the surface underneath the outflows generates vorticity, which may be advected into the frontal region, and may affect the dynamics of growing cumulus clouds. Also, the gravity waves generated by these density currents, though containing only a small amount of energy compared to that of the current itself, may in a conditionally unstable environment be sufficient to account for the triggering of convection ahead of the frontal boundary. We plan to explore both of these aspects in subsequent work.

Acknowledgments. This work was supported by the NSF Physical and Dynamical Meteorology program, Grant DYN078550. The computational component of this work was supported in part by the facilities and staff of the Yale University Faculty of Arts and Sciences High Performance Computing Center.

REFERENCES

Abe, S., and T. Yoshida, 1982: The effect of the width of a peninsula to the sea breeze. *J. Meteor. Soc. Japan,* **60,** 1074–1084.

Antonelli, M., and R. Rotunno, 2007: Large-eddy simulation of the onset of the sea breeze. *J. Atmos. Sci.,* **64,** 4445–4457.

Benjamin, T., 1968: Gravity currents and related phenomena. *J. Fluid Mech.,* **31,** 209–248.

Carbone, R. E., J. W. Wilson, T. D. Keenan, and J. M. Hacker, 2000: Tropical island convection in the absence of significant topography. Part I: Life cycle of diurnally forced convection. *Mon. Wea. Rev.,* **128,** 3459–3480.

Chemel, C., M. Russo, J. Pyle, and R. Sokhi, 2009: Quantifying the imprint of a severe Hector thunderstorm during ACTIVE/SCOUT-O3 onto the water content in the upper troposphere/lower stratosphere. *Mon. Wea. Rev.,* **137,** 2493–2514.

Crossman, E., and J. Horel, 2010: Sea and lake breezes: A review of numerical studies. *Bound.-Layer Meteor.,* **137,** 1–29.

Cunningham, R., 2007: Idealized numerical simulations of the interactions between buoyant plumes and density currents. *J. Atmos. Sci.,* **64,** 2105–2115.

Droegemeier, K., and R. Wilhelmson, 1987: Numerical simulation of thunderstorm outflow dynamics. Part I: Outflow sensitivity experiments and turbulence dynamics. *J. Atmos. Sci.,* **44,** 1180–1210.

Fovel, R., 2005: Convective initiation ahead of the sea-breeze front. *Mon. Wea. Rev.,* **133,** 264–278.

——, and P. Dailey, 2001: Numerical simulation of the interaction between the sea-breeze front and horizontal convective rolls. Part II: Alongshore ambient flow. *Mon. Wea. Rev.,* **129,** 2057–2072.

Gentilli, J., 1969: Some regional aspects of southerly buster phenomena. *Weather,* **24,** 173–184.

Grandpeix, J.-Y., and J.-P. Lafore, 2010: A density current parameterization coupled with Emanuel's convection scheme. Part I: The models. *J. Atmos. Sci.,* **67,** 881–897.

Haase, S., and R. Smith, 1989: The numerical simulation of atmospheric gravity currents. Part II. Environments with stable layers. *Geophys. Astrophys. Fluid Dyn.,* **46,** 35–51.

Haertel, P., R. Johnson, and S. Tulich, 2001: Some simple simulations of thunderstorm outflows. *J. Atmos. Sci.,* **58,** 504–516.

Hogg, A., M. Hallworth, and H. Huppert, 2005: On gravity currents driven by constant fluxes of saline and particle-laden fluid in the presence of a uniform flow. *J. Fluid Mech.,* **539,** 349–385.

Huppert, H., and J. Simpson, 1980: The slumping of gravity currents. *J. Fluid Mech.,* **99,** 785–799.

Keulegan, G. H., 1958: The motion of saline fronts in still water. National Bureau of Standards Rep. 5168, 29 pp.

Kingsmill, D., 1995: Convection initiation associated with a sea-breeze front, a gust front, and their collision. *Mon. Wea. Rev.,* **123,** 2913–2933.

Liu, C., and W. Moncrieff, 2000: Simulated density currents in idealized stratified environments. *Mon. Wea. Rev.,* **128,** 1420–1437.

Mahrer, Y., and M. Segal, 1985: On the effects of islands' geometry and size in inducing sea breeze circulation. *Mon. Wea. Rev.,* **113,** 170–174.

Maxworthy, T., J. Leilich, J. Simpson, and E. Meiburg, 2002: The propagation of a gravity current into a linearly stratified fluid. *J. Fluid Mech.,* **453,** 371–394.

Miller, S., B. Keim, R. Talbot, and H. Mao, 2003: Sea breeze: Structure, forecasting, and impacts. *Rev. Geophys.,* **41,** 1011, doi:10.1029/2003RG000124.

Moncrieff, W., and C. Liu, 1999: Convection initiation by density currents: Role of convergence, shear, and dynamical organization. *Mon. Wea. Rev.,* **127,** 2455–2464.

Mori, A., and H. Niino, 2002: Time evolution of nonlinear horizontal convection: Its flow regimes and self-similar solutions. *J. Atmos. Sci.,* **59,** 1841–1856.

Muir, L. C., and M. Reeder, 2010: Idealized modelling of land-falling cold fronts. *Quart. J. Roy. Meteor. Soc.,* **136,** 2147–2161.

Reeder, M., 1986: The interaction of a surface cold front with a prefrontal thermodynamically well-mixed boundary layer. *Aust. Meteor. Mag.,* **34,** 137–148.

Robinson, F., S. Sherwood, and Y. Li, 2008: Resonant response of deep convection to surface hot spots. *J. Atmos. Sci.,* **65,** 276–286.

——, ——, D. Gerstle, C. Liu, and D. Kirshbaum, 2011: Exploring the land–ocean contrast in convective vigor using islands. *J. Atmos. Sci.,* **68,** 602–618.

Rottman, J. W., and J. E. Simpson, 1983: Gravity currents produced by instantaneous releases of a heavy fluid in a rectangular channel. *J. Fluid Mech.,* **135,** 95–110.

Rotunno, R., 1983: On the linear theory of the land and sea breeze. *J. Atmos. Sci.,* **40,** 1999–2009.

——, J. Klemp, G. Bryan, and D. Muraki, 2011: Models of non-Boussinesq lock-exchange flow. *J. Fluid Mech.,* **675,** 1–26.

Savijarvi, H., and S. Matthews, 2004: Flow over small heat islands: A numerical sensitivity study. *J. Atmos. Sci.,* **61,** 859–868.

Seigel, R. B., and S. C. van den Heever, 2012: Simulated density currents beneath embedded stratified layers. *J. Atmos. Sci.,* **69,** 2192–2200.

Sha, W., and T. Kawamura, 1991: A numerical study on sea/land breezes as a gravity current: Kelvin–Helmholtz billows and inland penetration of the sea-breeze front. *J. Atmos. Sci.,* **48,** 1649–1665.

Shin, J., S. Dalziel, and P. Linden, 2004: Gravity currents produced by lock exchange. *J. Fluid Mech.,* **521,** 1–34.

Skamarock, W., and Coauthors, 2008: A description of the advanced research WRF version 3. NCAR Tech. Note NCAR/TN475+STR, 113 pp.

Smith, R., and M. Reeder, 1988: On the movement and low-level structure of cold fronts. *Mon. Wea. Rev.,* **116,** 1927–1944.

Soong, S.-T., and Y. Ogura, 1980: Response of tradewind cumuli to large-scale processes. *J. Atmos. Sci.,* **37,** 2035–2050.

Thomsen, G. L., M. J. Reeder, and R. K. Smith, 2008: The diurnal evolution of cold fronts in the Australian subtropics. *Quart. J. Roy. Meteor. Soc.,* **135,** 395–411.

Ungarish, M., 2009: *An Introduction to Gravity Currents and Intrusions.* Chapman and Hall/CRC Press, 512 pp.

von Kármán, T., 1940: The engineer grapples with nonlinear problems. *Bull. Amer. Math. Soc.,* **46,** 615–683.

Wicker, L., and W. Skamarock, 2002: Time splitting methods for elastic models using forward schemes. *Mon. Wea. Rev.,* **130,** 2088–2097.

Wu, C.-M., B. Stevens, and A. Arakawa, 2009: What controls the transition from shallow to deep convection? *J. Atmos. Sci.,* **66,** 1793–1806.

Xian, Z., and R. Pielke, 1991: The effects of width of landmasses on the development of sea breezes. *J. Appl. Meteor.,* **30,** 1280–1304.